Asociación Argentina
de Mecánica Computacional

Mecánica Computacional Vol XXXIII, págs. 1407-1419 (artículo completo)
Graciela Bertolino, Mariano Cantero, Mario Storti y Federico Teruel (Eds.)
San Carlos de Bariloche, 23-26 Setiembre 2014

DISCONTINUOUS BIFURCATION ANALYSIS IN MICROPLANES THEORY

Sonia M. Vrech[1] **and Guillermo Etse**[1]

[1]*CEMNCI, CONICET, Center for Numerical and Computational Methods in Engineering, Faculty for Exact Sciences and Technology, National University of Tucuman, Argentina*

Keywords: Microplanes, discontinuous bifurcation, concrete.

Abstract. Conditions for discontinuous bifurcation in limit states of thermodynamically consistent microplane theory for cohesive-frictional materials like concrete are evaluated by means of analytical methods. Explicit solutions for brittle failure conditions in the form of discontinuous bifurcation are proposed. Numerical analysis are comparatively assessed for different limit stress states regarding both microplane and macroscopic response. Macroscopic critical values are computed by analytical and geometrical methods. The results in this work illustrate the capabilities of the thermodynamically consistent microplane theory to reproduce localized failure modes in uniaxial tension, uniaxial compression and simple shear regimes of cohesive-frictional materials like concrete.

1 INTRODUCTION

The term *localization* refers to the formation of restricted failure zones with high concentration of deformations while the rest of the structure might even exhibit unloading. The failure process begins with the formation of micro-cracks and micro-voids whose accumulation with progressive load results in zones of strongly localized distortions. Quasi-brittle materials like concretes and soils exhibit spatial discontinuities of the kinematic fields when they are sufficiently deformed into the inelastic regime conducing to highly anisotropic material response (Kuhl et al. (2000)).

It becomes necessary to distinguish failure mechanisms that characterize tension, compression and shear regimes. Failure mechanism in tensile regime is fully controlled by the fracture energy release process in one single crack while the material outside the crack remains practically undamaged and subjected to elastic unloading, see a.o. Planas and Elices (1986, 1989); Guo and Zhang (1987); Phillips and Binsheng (1993); Etse and Willam (1994). While in compressive regime the failure mechanism is characterized by both the appearance of several micro-cracks in the normal direction to the local maximum principal stress and the evolution of damage processes in zones located in between cracks or micro-cracks, see a.o. Hurlbut (1985); van Geel (1998); Sfer et al. (2002); Lu (2005); van Mier (1984).

Localized failure mechanisms on quasi-brittle materials, depending on governing stresses as well as mechanical and chemical features, have been experimentally observed by a. o. Vardoulakis (1980); Petersson (1981); Oda and Kazama (1988); Ehlers and Volk (1997); van Mier (1997).

From the analytical point of view, regarding smeared-crack theories for constitutive modelling of engineering materials, it is possible the mathematical evaluation of brittle or localized failure modes described by means of discontinuous bifurcations or jumps in the velocity gradients. After the original works by Hadamard (1903); Nadai (1950); Thomas (1961); Hill (1962); Rudnicki and Rice (1975), many authors have studied the problem in a systematic manner developing mathematical conditions and indicators that signalize the initiation of localized failure modes in the form of discontinuous bifurcation, see a.o. Sobh (1987); Perić (1990); Willam and Etse (1990); Ottosen and Runesson (1991); Rizzi and Willam (1995); Pijaudier-Cabot and Benallal (1993); Jirásek and Rolshoven (2009); Vrech and Etse (2006).

The present work is focused on the comparison of the localized failure characteristics of the well-known macroscopic Drucker-Prager plasticity formulation with the microplane-based one with the aim to demonstrate the capabilities of the microplane theory to reproduce localized failure modes.

In first place, constitutive equations of the thermodynamically consistent macroscopic plasticity model are summarized. After a brief description of the analytical discontinuous bifurcation conditions, the geometrical interpretation is deduced. Later, thermodynamically consistent microplane-based plasticity model is developed and localized failure properties in terms of discontinuous bifurcation are analyzed. Critical directions in macro and micro-plasticity frameworks of limit stress states corresponding to tension, compression and shear regimes are compared.

2 THERMODYNAMICALLY CONSISTENT MACROSCOPIC ELASTO-PLATICITY

Starting from the additive decomposition of the strain tensor $\boldsymbol{\varepsilon} = \boldsymbol{\nabla}^{sym}\boldsymbol{u}$ into the elastic and plastic components

$$\boldsymbol{\varepsilon} = \boldsymbol{\varepsilon}^e + \boldsymbol{\varepsilon}^p \tag{1}$$

and the definition of a macroscopic free energy potential Ψ^{mac} in terms of the elastic strain tensor and the internal variable κ in case of isotropic plasticity

$$\Psi^{mac}(\boldsymbol{\varepsilon}^e, \kappa) = \frac{1}{2}\boldsymbol{\varepsilon}^e : \boldsymbol{E}^e : \boldsymbol{\varepsilon}^e + \int_0^\kappa \phi(\kappa) d\kappa \tag{2}$$

being $\boldsymbol{E}^e$ the fourth order elastic tensor, from the Clausius-Duhem inequality the expressions for the stress tensor $\boldsymbol{\sigma}$ and yield stress ϕ^{mac} result

$$\begin{aligned} \boldsymbol{\sigma} &= \frac{\partial \Psi^{mac}}{\partial \boldsymbol{\varepsilon}^e} \quad \Rightarrow \quad \dot{\boldsymbol{\sigma}} = \boldsymbol{E}^e : [\dot{\boldsymbol{\varepsilon}} - \dot{\boldsymbol{\varepsilon}^p}] \\ \phi^{mac} &= \frac{\partial \Psi^{mac}}{\partial \kappa} \quad \Rightarrow \quad \dot{\phi}^{mac} = \bar{H}\dot{\kappa} \end{aligned} \tag{3}$$

being $\bar{H}$ the hardening/softening modulus.

A convex yield function $\Phi^{mac}(\boldsymbol{\sigma}, \phi^{mac}) \leq 0$ and a plastic potential $\Phi^{*mac}(\boldsymbol{\sigma}, \phi^{mac}) \leq 0$ that differs is the non-associated case are defined, being its normal vectors

$$\boldsymbol{\nu} = \frac{\partial \Phi^{mac}}{\partial \boldsymbol{\sigma}} \quad \text{and} \quad \boldsymbol{\mu} = \frac{\partial \Phi^{*mac}}{\partial \boldsymbol{\sigma}} \tag{4}$$

respectively. The evolution of the loading surfaces is governed by the plastic strain tensor rate

$$\dot{\boldsymbol{\varepsilon}}^p = \dot{\lambda}\boldsymbol{\mu} \tag{5}$$

and satisfies the Kuhn-Tucker conditions

$$\Phi^{mac} \leq 0 \quad , \quad \dot{\lambda} \geq 0 \quad , \quad \Phi^{mac}\dot{\lambda} = 0 \tag{6}$$

as well as the consistency condition $\dot{\Phi}^{mac}\dot{\lambda} = 0$, from which it is possible to deduce the plastic parameter rate $\dot{\lambda}$ to obtain the analytical expression for the elasto-plastic tangent material operator

$$\boldsymbol{E}^{ep} = \frac{\partial \boldsymbol{\sigma}}{\partial \boldsymbol{\varepsilon}} = \boldsymbol{E}^e - \frac{1}{h}\boldsymbol{E}^e : \boldsymbol{\mu} \otimes \boldsymbol{\nu} : \boldsymbol{E}^e \quad , \quad h = \boldsymbol{\nu} : \boldsymbol{E}^e : \boldsymbol{\mu} + \bar{H} \tag{7}$$

3 ANALYTICAL SOLUTION FOR LOCALIZED FAILURE

In the realm of the smeared crack approach, localized failure modes are related to discontinuous bifurcations of the equilibrium path, and lead to lost of ellipticity of the equations that govern the static equilibrium problem. The inhomogeneous or localized deformation field exhibits a plane of discontinuity that can be identified by means of the eigenvalue problem of the acoustic or localization tensor, see a.o. Ottosen and Runesson (1991) and Willam and Etse (1990). Analytical solutions for the discontinuous bifurcation condition based on original works by Hadamard (1903); Thomas (1961); Hill (1962) are described in this section.

Firstly, the jump of the gradient displacement rate is expressed according Maxwell's compatibility condition

$$[|\boldsymbol{\nabla}\dot{\boldsymbol{u}}|] = \xi \boldsymbol{m} \otimes \boldsymbol{n} \quad \longrightarrow \quad [|\dot{\boldsymbol{\varepsilon}}|] = \xi [\boldsymbol{m} \otimes \boldsymbol{n}]^{sym} \tag{8}$$

being ξ de jump amplitude, $\boldsymbol{m}$ the unit jump vector and $\boldsymbol{n}$ the unit normal vector to the failure surface.

Moreover, the equilibrium condition of the traction vectors across the discontinuity surface $\boldsymbol{t} = \boldsymbol{n} \cdot \boldsymbol{\sigma}$ states

$$[|\dot{\boldsymbol{t}}|] := \dot{\boldsymbol{t}}^{+} - \dot{\boldsymbol{t}}^{-} = \boldsymbol{0} \quad \longrightarrow \quad [|\dot{\boldsymbol{t}}|] = \boldsymbol{n} \cdot [|\dot{\boldsymbol{\sigma}}|] = \boldsymbol{n} \cdot [|\boldsymbol{E}^{ep} : \dot{\boldsymbol{\varepsilon}}|] = \boldsymbol{0} \tag{9}$$

Substituting Eq. (8-b) in (9-b) the localization condition is obtained and expressed as

$$\xi \boldsymbol{Q}^{ep} \cdot \boldsymbol{m} = 0 \quad , \quad \boldsymbol{Q}^{ep} := \boldsymbol{n} \cdot \boldsymbol{E}^{ep} \cdot \boldsymbol{n} \tag{10}$$

being $\boldsymbol{Q}^{ep}$ the elasto-plastic localization or acoustic tensor. The necessary condition for the onset of localization indicating the loss of ellipticity is characterized by the singularity condition of the acoustic tensor

$$det(\boldsymbol{Q}^{ep}) = 0 \tag{11}$$

It leads to the analysis of the spectral properties of the tensor defined as

$$\boldsymbol{Q}^{ep} = \boldsymbol{Q}^{e} - \frac{1}{h} \boldsymbol{a}^{*} \otimes \boldsymbol{a} \quad , \quad \boldsymbol{Q}^{e} := \boldsymbol{n} \cdot \boldsymbol{E}^{e} \cdot \boldsymbol{n} \tag{12}$$

being $\boldsymbol{Q}^{e}$ the elastic localization tensor. The smallest eigenvalue of $\boldsymbol{Q}^{ep}$ with respect to the metric defined by $[\boldsymbol{Q}^{e}]^{-1}$ is

$$\lambda^{(1)} = 1 - \frac{\boldsymbol{a}(\boldsymbol{n}) \cdot [\boldsymbol{Q}^{e}(\boldsymbol{n})]^{-1} \cdot \boldsymbol{a}^{*}(\boldsymbol{n})}{h} = 0 \tag{13}$$

with the vectors $\boldsymbol{a}$ and $\boldsymbol{a}^{*}$ defined as

$$\boldsymbol{a} = \boldsymbol{\nu} : \boldsymbol{E}^{e} \cdot \boldsymbol{n} \quad , \quad \boldsymbol{a}^{*} = \boldsymbol{n} \cdot \boldsymbol{E}^{e} : \boldsymbol{\mu} \tag{14}$$

By replacing Eq. (7-b) in (13), the necessary condition for localization and the corresponding critical hardening/softening modulus $\bar{H}_c$ is obtained

$$\bar{H}_c + \boldsymbol{\nu} : \boldsymbol{E}^{e} : \boldsymbol{\mu} - \boldsymbol{a} \cdot [\boldsymbol{Q}^{ep}]^{-1} \cdot \boldsymbol{a}^{*} = 0 \tag{15}$$

3.1 GEOMETRICAL INTERPRETATION

The approach follows the original proposal by Benallal (1992), which was further developed by a.o. Pijaudier-Cabot and Benallal (1993), Benallal and Comi (1996), Liebe and Willam (2001) for classical plasticity.

The localization condition in Eq. (15) defines an ellipse

$$\frac{(\sigma - \sigma_0)^2}{A^2} - \frac{\tau^2}{B^2} = 1 \tag{16}$$

in the $\sigma - \tau$ Mohr's coordinates

$$\sigma = \boldsymbol{n} \cdot \boldsymbol{\sigma} \cdot \boldsymbol{n} \quad , \quad s = \boldsymbol{n} \cdot \boldsymbol{S} \cdot \boldsymbol{n} \tag{17}$$

$$\tau^2 = (\boldsymbol{n} \cdot \boldsymbol{S}) \cdot (\boldsymbol{n} \cdot \boldsymbol{S}) - (\boldsymbol{n} \cdot \boldsymbol{S} \cdot \boldsymbol{n})^2 \tag{18}$$

being $\boldsymbol{S}$ the deviatoric stress tensor and $\boldsymbol{n}$ the normal to the plane where the Mohr components are evaluated. The localization ellipse and Mohr's circle parameters are shown in Fig. 1.

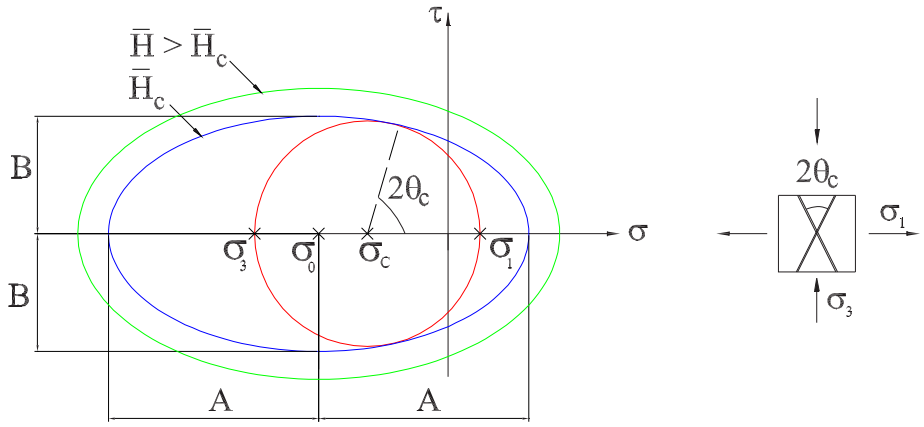

Figure 1: Mohr's circle and localization ellipse.

The tangency between the largest Mohr's circle of stresses and the geometric representation of Eq. (15) determines the geometrical localization condition. The maximum hardening/softening parameter $\bar{H}_c$ and the critical directions for localization θ_c, are obtained when the Mohr's circle of stresses

$$(\sigma - \sigma_c)^2 + \tau^2 = R^2 \tag{19}$$

contacts the elliptical localization envelope. The center and radius are computed as

$$\sigma_c = \frac{\sigma_1 + \sigma_3}{2} \quad \text{and} \quad R = \frac{\sigma_1 - \sigma_3}{2} \tag{20}$$

with σ_1 and σ_3 the major and minor principal stresses, respectively.

According to Liebe (1998) three different failure modes may be distinguished depending on the contact points location: mode I, mode II and mixed mode.

The critical failure directions for localization θ_c, obtained from the tangential contact between the elliptical localization envelope of Eq. (16) and the major Mohr's circle of Eq. (19), are deduced from

$$\tan^2(\theta_c) = \frac{R - (\sigma_c - \sigma_0)/(d^2 - 1)}{R + (\sigma_c - \sigma_0)/(d^2 - 1)} \quad ; \quad d^2 = \frac{A^2}{B^2} \tag{21}$$

4 DRUCKER-PRAGER PLASTICITY

The expressions of the second order Drucker-Prager yield criterium (see Drucker and Prager (1952)) and the adopted plastic potential have the form

$$\begin{aligned} \Phi^{mac} &= J_2 + \alpha_F^{mac} I_1 - \phi^{mac} = 0 \\ \Phi^{*mac} &= J_2 + \alpha_Q^{mac} I_1 - \phi^{mac} = 0 \end{aligned} \tag{22}$$

being I_1 the first invariant of the stress tensor $\boldsymbol{\sigma}$ and J_2 the second invariant of the deviator stress tensor $\boldsymbol{S}$. The parameters α_F^{mac} and ϕ^{mac} represent the friction angle and yield stress,

respectively. Expressed in terms of the uniaxial compressive and tensile strength f_c and f_t, they result

$$\alpha_F^{mac} = \frac{f_c - f_t}{3} \quad , \quad \phi^{mac} = \frac{f_c f_t}{3} \tag{23}$$

whereas $\alpha_Q^{mac} = \eta \alpha_F^{mac}$ corresponds to the dilatancy angle, being η the non-associated coefficient.

Normal vectors to the yield and plastic potential surfaces are expressed as

$$\begin{aligned} \boldsymbol{\nu} &= \boldsymbol{S} + \alpha_F^{mac} \boldsymbol{I} \\ \boldsymbol{\mu} &= \boldsymbol{S} + \alpha_Q^{mac} \boldsymbol{I} \end{aligned} \tag{24}$$

4.1 LOCALIZATION ANALISYS OF DRUCKER-PRAGER PLASTICITY

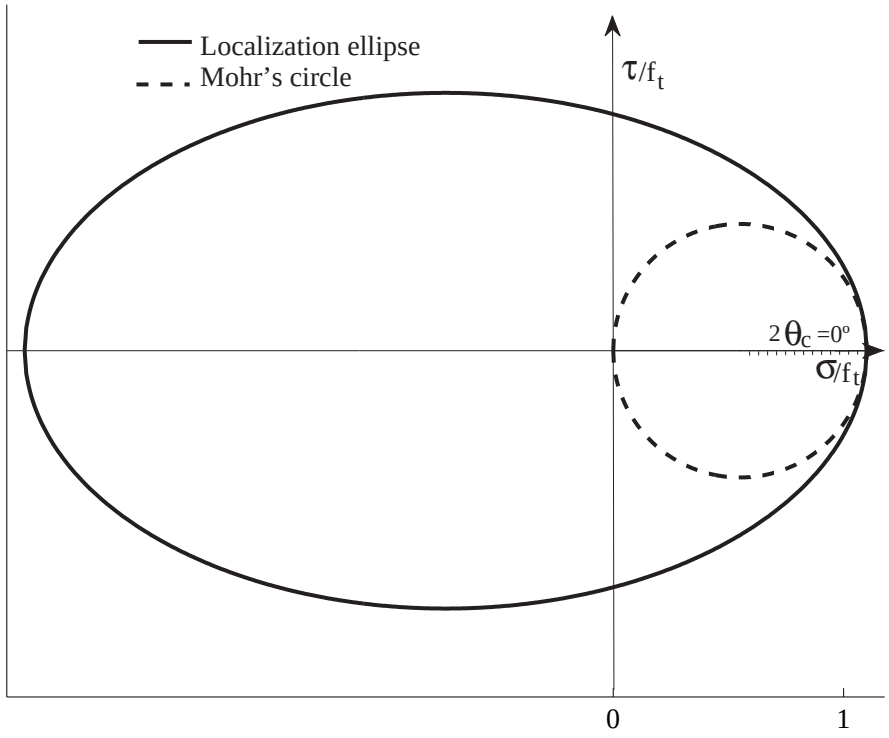

Figure 2: Localization ellipse for uniaxial tension test.

Localization properties of the thermodynamically consistent Drucker-Prager plasticity for the plane strain state when $\sigma_z = \nu(\sigma_x + \sigma_y)$ where published by the authors, see Vrech and Etse (2006). Critical localization directions as well as critical hardening/softening parameter for different strength ratios f_c/f_t and Poisson's modulus were computed by both analytical and geometrical methods for different limit stress states.

In this section, considering the following material properties:

Elastic modulus - E= 19305.3 MPa

Poisson's ratio - ν= 0.2

Compressive strength - f_c= 22.0 MPa

Tensile strength - f_t= 2.75 MPa

Non-associated coefficient - η= 0

localization ellipses and Mohr's circles corresponding to the limit stress states of uniaxial tension, uniaxial compression and simple shear tests are shown in Figs. 2 to 6. Obtained critical directions given by curves tangency are computed as:

θ_c= 0° and 180° for uniaxial tension;

θ_c= 31.5° and 148.5° for uniaxial compression; and

θ_c= 15.75° and 164.25° for simple shear test.

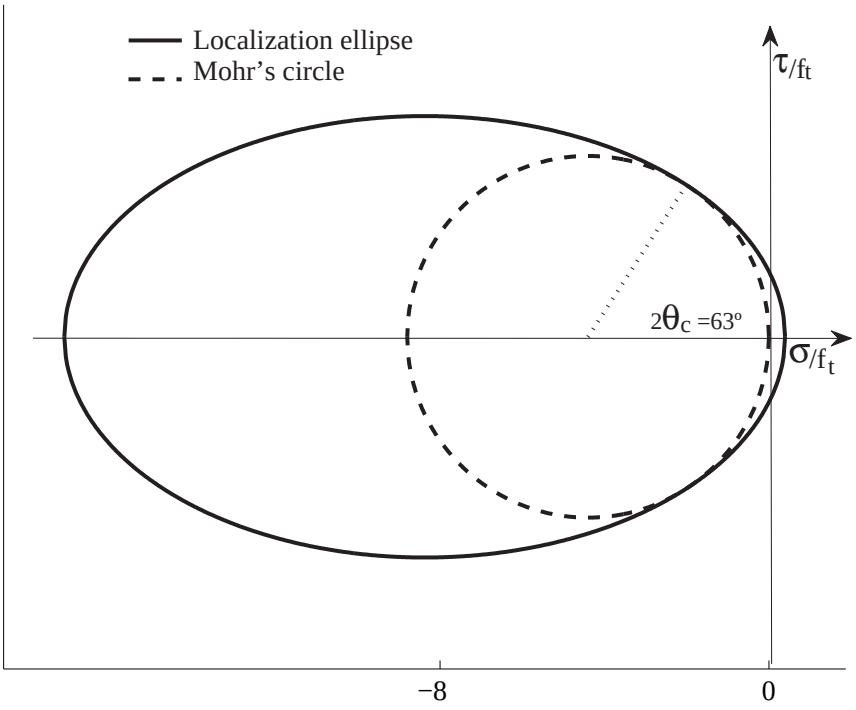

Figure 3: Localization ellipse for uniaxial compression test.

5 MICROPLANE-BASED ELASTO PLASTICITY

This formulation is based on the thermodynamically consistent approach for the derivation of macroscopic stresses and equilibrium equations given by Carol et al. (2001) and Kuhl et al. (2001) for the case of isotropic plasticity.

Assuming kinematic constraints, scalar volumetric strain and tangential strain vector at microplane level (ε_V and $\boldsymbol{\varepsilon}_T$, respectively) are computed by means the following relationships

$$\varepsilon_V = \boldsymbol{V} : \boldsymbol{\varepsilon} \quad , \quad \boldsymbol{\varepsilon}_T = \boldsymbol{T} : \boldsymbol{\varepsilon} \tag{25}$$

being $\boldsymbol{\varepsilon}$ the macroscopic strain tensor projected on a microplane of normal direction $\boldsymbol{n}$, see Fig. 5. The projection tensors are defined as

$$\boldsymbol{V} = \frac{1}{3}\boldsymbol{I} \quad , \quad \boldsymbol{T} = \boldsymbol{n} \cdot I^{sym} - \boldsymbol{n} \otimes \boldsymbol{n} \otimes \boldsymbol{n} \tag{26}$$

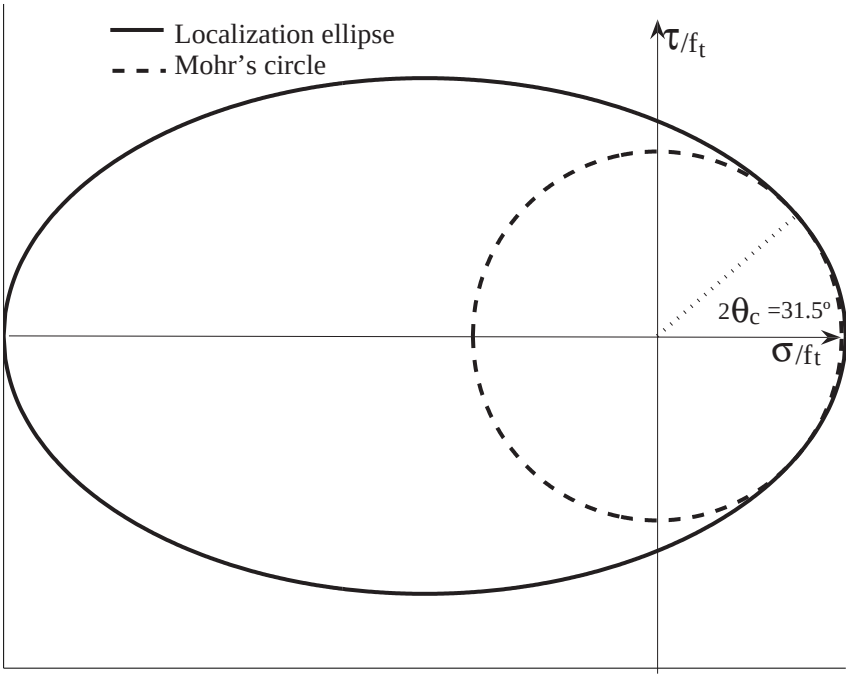

Figure 4: Localization ellipse for simple shear test.

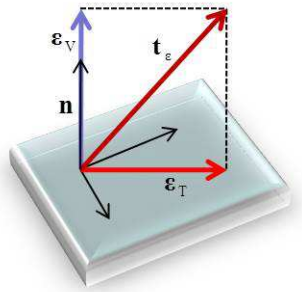

Figure 5: Strain components at the microplane level.

The strain vector at microplane level results

$$\boldsymbol{t}_\varepsilon = \varepsilon_V \boldsymbol{n} + \boldsymbol{\varepsilon}_T \tag{27}$$

Assuming the macro free-energy potential as the integral of the micro free-energy on a spherical region of unit volume Ω, the following micro-macro free-energy relationship is proposed

$$\psi^{mac} = \frac{3}{4\pi} \int_{\Omega} \psi^{mic} \mathrm{d}\Omega \tag{28}$$

being ψ^{mic}=$\psi^{mic}(\varepsilon_V, \boldsymbol{\varepsilon}_T, \kappa)$ the free-energy potential at microplane level, expressed in terms of

the strain components and the scalar internal variable. Assuming small strains and regarding the additive decomposition of the macroscopic strain tensor of Eq. (1), the microscopic strain components are expressed as

$$\varepsilon_V = \varepsilon_V^e + \varepsilon_V^p \quad , \quad \boldsymbol{\varepsilon}_T = \boldsymbol{\varepsilon}_T^e + \boldsymbol{\varepsilon}_T^p \tag{29}$$

Constitutive micro-stresses are computed as

$$\begin{aligned} \sigma_V := \frac{\partial \psi^{mic}}{\partial \varepsilon_V} \quad &\rightarrow \quad \dot{\sigma}_V = E_V^e[\dot{\varepsilon}_V - \dot{\varepsilon}_V^p] \\ \boldsymbol{\sigma}_T := \frac{\partial \psi^{mic}}{\partial \boldsymbol{\varepsilon_T}} \quad &\rightarrow \quad \dot{\boldsymbol{\sigma}}_T = E_T^e[\dot{\boldsymbol{\varepsilon}}_T - \dot{\boldsymbol{\varepsilon}}_T^p] \end{aligned} \tag{30}$$

while the dissipative stresses can be computed at microplane level as

$$\phi^{mic} = \frac{\partial \psi^{mic}}{\partial \kappa} \quad \rightarrow \quad \dot{\phi}^{mic} = \bar{H}\dot{\kappa} \tag{31}$$

As in case of macroscopic plasticity, both yield and plastic potential surfaces are set as

$$\begin{aligned} \Phi^{mic}(\sigma_V, \boldsymbol{\sigma}_T, \phi^{mic}) \leq 0 \quad \text{with} \quad \nu_V = \frac{\partial \Phi^{mic}}{\partial \sigma_V} \quad \text{and} \quad \boldsymbol{\nu}_T = \frac{\partial \Phi^{mic}}{\partial \boldsymbol{\sigma}_T} \\ \Phi^{*mic}(\sigma_V, \boldsymbol{\sigma}_T, \phi^{mic}) \leq 0 \quad \text{with} \quad \mu_V = \frac{\partial \Phi^{*mic}}{\partial \sigma_V} \quad \text{and} \quad \boldsymbol{\mu}_T = \frac{\partial \Phi^{*mic}}{\partial \boldsymbol{\sigma}_T} \end{aligned} \tag{32}$$

and the evolution of the plastic strain components yields

$$\dot{\varepsilon}_V^p = \dot{\lambda}\mu_V \quad , \quad \dot{\boldsymbol{\varepsilon}}_T^p = \dot{\lambda}\boldsymbol{\mu}_T \quad , \quad \dot{\kappa} = \dot{\lambda} \tag{33}$$

regarding the Kuhn-Tucker conditions of Eq. (6) and the consistency condition.

The homogenization of the microplanes energy of Eq. (28) leads to the definition of the macroscopic stress tensor

$$\boldsymbol{\sigma} = \frac{\partial \psi^{mac}}{\partial \boldsymbol{\varepsilon}} = \frac{3}{4\pi}\int_\Omega \boldsymbol{V}\sigma_V + \boldsymbol{T}^T \cdot \boldsymbol{\sigma}_T d\Omega \tag{34}$$

The analytical evaluation of this integral can be solved by numerical integration techniques proposed by Bažant and Oh (1986) .

The macroscopic tangent operator can be analogously obtained as

$$E^{ep} = \frac{d\boldsymbol{\sigma}}{d\boldsymbol{\varepsilon}} = \frac{3}{4\pi}\int_\Omega \left[\boldsymbol{V} \otimes \frac{d\boldsymbol{\sigma}}{d\varepsilon_V} + \boldsymbol{T}^T \cdot \frac{d\boldsymbol{\sigma}}{d\boldsymbol{\varepsilon}_T}\right] d\Omega \tag{35}$$

resulting

$$E^{ep} = E^e - \frac{3}{4\pi}\int_\Omega \frac{1}{h}\left[E_V^e \boldsymbol{V}\mu_V + E_T^e \boldsymbol{T}^T \cdot \boldsymbol{\mu}_T\right] \otimes \left[\nu_V \boldsymbol{V} E_V^e + \boldsymbol{\nu}_T \cdot \boldsymbol{T}^T E_T^e\right] d\Omega \tag{36}$$

with the elastic macroscopic tangent operator computed as

$$E^e = \frac{3}{4\pi}\int_\Omega E_V^e \boldsymbol{V} \otimes \boldsymbol{V} + E_T^e \boldsymbol{T}^T \cdot \boldsymbol{T} d\Omega \tag{37}$$

5.1 MICROPLANE-BASED DRUCKER-PRAGER PLASTICITY

The relationship between microplane-based parameters and macroscopic ones for isotropic elasticity has been established by Kuhl et al. (2000) as

$$E_V^e = 3K \quad \text{and} \quad E_V^e = \frac{10}{3}G \tag{38}$$

being K and G the compressive and shear modules, respectively. Whereas the first invariant of the macroscopic strain tensor can be expressed as

$$I_1 = \boldsymbol{\varepsilon} : \boldsymbol{I} = \frac{3}{4\pi}\int_\Omega \varepsilon_V d\Omega \tag{39}$$

and the second invariant of macroscopic strain deviator as

$$J_2 = \frac{1}{2}\boldsymbol{\varepsilon}^{dev} : \boldsymbol{\varepsilon}^{dev} = \frac{3}{4\pi}\int_\Omega \frac{3}{10}\boldsymbol{\varepsilon}_T \cdot \boldsymbol{\varepsilon}_T d\Omega \tag{40}$$

In the elastic regime, the same relationships hold for macroscopic stress invariants

$$I_1 \approx \frac{3}{4\pi}\int_\Omega \sigma_V d\Omega \quad \text{and} \quad J_2 \approx \frac{3}{4\pi}\int_\Omega \frac{3}{10}\boldsymbol{\sigma}_T \cdot \boldsymbol{\sigma}_T d\Omega \tag{41}$$

The microplane-based friction coefficient and yield stress must be related to their macroscopic counterparts. With this aim the parabolic Drucker-Prager yield function of Eq. (22-a) is rewritten as

$$\Phi^{mac} \approx \frac{3}{4\pi}\int_\Omega \left[\frac{3}{10}\boldsymbol{\sigma}_T \cdot \boldsymbol{\sigma}_T + \frac{f_c - f_t}{3}\sigma_V - \frac{1}{3}\frac{f_c f_t}{3}\right] d\Omega \tag{42}$$

whereas the microplane-based yield function as

$$\Phi^{mic} = \frac{1}{2}\boldsymbol{\sigma}_T \cdot \boldsymbol{\sigma}_T + \alpha_F^{mic}\sigma_V - \phi^{mic} = 0 \tag{43}$$

From the comparison between last equations arises

$$\alpha^{mic} \approx \frac{5}{3}\frac{f_t - f_c}{3} \quad \text{and} \quad \phi^{mic} \approx \frac{5}{9}\frac{f_c f_t}{3} \tag{44}$$

5.2 MICROPLANE-BASED LOCALIZATION ANALISYS OF DRUCKER-PRAGER PLASTICITY

The macroscopic localization condition of Eq. (11), can be rewritten for the case of microplane-based plasticity as

$$det(\boldsymbol{Q}^{ep}) = 0 \quad \text{with} \quad \boldsymbol{Q}^{ep} = \boldsymbol{Q}^e - \frac{3}{4\pi}\int_\Omega \frac{\boldsymbol{a}^* \otimes \boldsymbol{a}}{h} d\Omega \tag{45}$$

with the traction vectors computed as

$$\begin{aligned} \boldsymbol{a} &= [\nu_V \boldsymbol{V} E_V^e + \boldsymbol{\nu}_T \cdot \boldsymbol{T} E_T^e] \cdot \boldsymbol{n} \\ \boldsymbol{a}^* &= \boldsymbol{n} \cdot [E_V^e \boldsymbol{V} \mu_V + E_T^e \boldsymbol{T} \cdot \boldsymbol{\mu}_T] \end{aligned} \tag{46}$$

and

$$h = \bar{H} + \nu_V E_V^e \mu_V + \boldsymbol{\nu}_T E_T^e \cdot \boldsymbol{\mu}_T \tag{47}$$

Normal vectors to the micro-yield surface and plastic potential are computed as

$$\begin{aligned} \nu_V &= \frac{\partial \Phi^{mic}}{\partial \sigma_V} = \alpha^{mic} \quad \text{and} \quad \boldsymbol{\nu}_T = \frac{\partial \Phi^{mic}}{\partial \boldsymbol{\sigma}_T} = \boldsymbol{\sigma}_T \\ \mu_V &= \frac{\partial \Phi^{*mic}}{\partial \sigma_V} = \alpha^{*mic} \quad \text{and} \quad \boldsymbol{\mu}_T = \frac{\partial \Phi^{*mic}}{\partial \boldsymbol{\sigma}_T} = \boldsymbol{\sigma}_T \end{aligned} \tag{48}$$

Due to the complex structure of the acoustic tensor for microplane-based plasticity in Eq. (45), analytical assessment becomes impossible. Numerical solutions are applied to compare localization results with those corresponding to macroscopic analysis in Section 4.1.

The results in Fig. 6 show normalized values of $det(Q^{ep})/det(Q^{e})$ for microplane-based Drucker-Prager plasticity. Critical directions for limit stress states of uniaxial tension, uniaxial compression and simple shear test are evaluated. The obtained results:

θ_c= 0° and 180° for uniaxial tension and simple shear tests; and

θ_c= 31.5° and 148.5° for uniaxial compression test

demonstrate comparable response behavior and localized failure modes for the three cases.

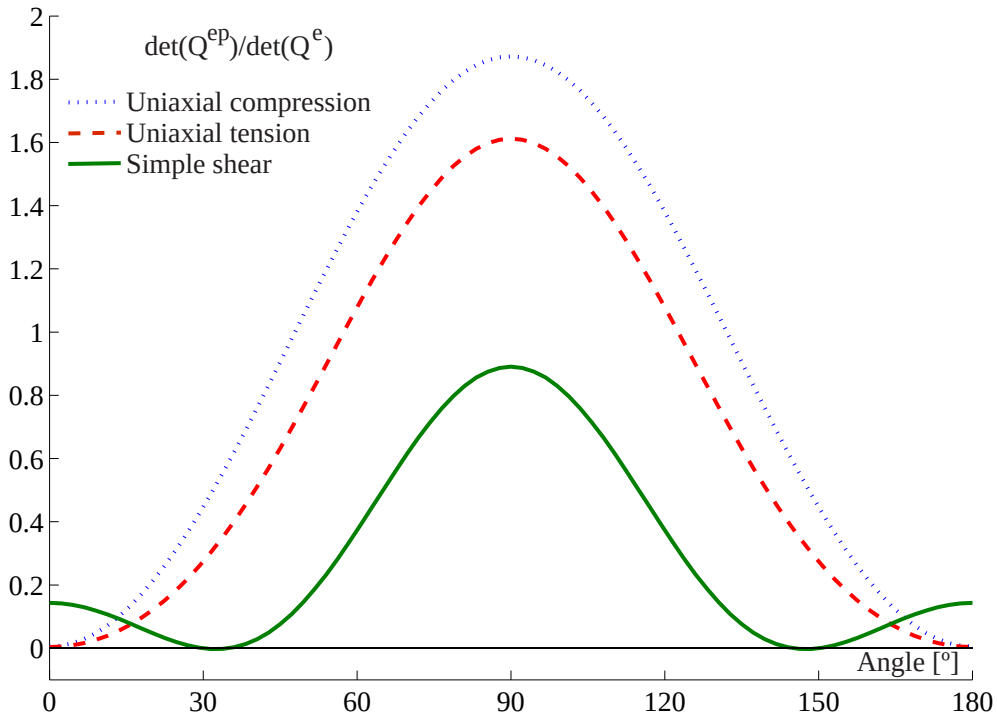

Figure 6: Bifurcation analysis for microplane-based Drucker-Prager platicity.

6 CONCLUSIONS

In this work, numerical conditions for discontinuous bifurcation in limit states of thermodynamically consistent microplane theory for cohesive-frictional materials like concrete were evaluated.

The microplane based-elastoplastic localization condition was expressed in terms of the singularity of the acoustic tensor, obtained through integration of non-linear material processes on each microplane over all posible orientations.

Then, for limit stress sates in simple traction, compression and shear regimes, critical localization directions were evaluated

The results in this work illustrate the capabilities of the thermodynamically consistent microplane plasticity to reproduce localized failure modes an critical directions comparable with those of macroscopic formulations.

REFERENCES

Bažant Z. and Oh B. Efficient numerical integration on the surface of a sphere. *ZAMM*, 66:37–49, 1986.

Benallal A. On localization phenomena in thermo-elasto-plasticity. *Arch. Mech.*, 44:15–29, 1992.

Benallal A. and Comi C. Localization analysis via a geometrical method. *International Journal of Solids and Structures*, 33:99–119, 1996.

Carol I., Jirasek M., and Bažant Z. A thermodynamically consistent approach to microplane theory. Part I. free-energy and consistent microplane stresses. *International Journal of Solids and Structures*, 38, 2001.

Drucker D. and Prager W. Soil mechanics and plastic analysis of limit design. *Quart. Appl. Math.*, 10:157–175, 1952.

Ehlers W. and Volk W. On shear band localization phenomena of liquid-saturated granular elastoplastic porous solid material accounting for viscosity and micropolar solid rotations. *Mech. Frict. Mat.*, 2:301–320, 1997.

Etse G. and Willam K. A fracture energy-based constitutive theory for inelastic behavior of plain concrete. *ACI Mater. J.*, 120, 1994.

Guo Z. and Zhang X. Investigation of complete stress-deformation curves for concrete in tension. *ACI Mater. J.*, 84:278–285, 1987.

Hadamard J. *Propagation des ondes et les equations d'Hydrodynamique*. New York. Chelsea, 1903.

Hill R. Acceleration waves in solids. *J. Mech. of Phys. and Sol.*, pages 1–16, 1962.

Hurlbut B. *Experimental and computational investigation of strain-softening in concrete*. Master's thesis, University of Colorado, 1985.

Jirásek M. and Rolshoven S. Localization properties of strain-softening gradient plasticity models. Part I: Srain-gradient theories. *International Journal of Solids and Structures*, 46:2225–2238, 2009.

Kuhl E., Ramm E., and Willam K. Finite differences and finite volumes. Two old friends. *International Journal of Solids and Structures*, 37:7259–7280, 2000.

Kuhl E., Steinmann P., and Carol I. A thermodynamically consistent approach to microplane theory. part ii. dissipation and inelastic constitutive modeling. *International Journal of Solids and Structures*, 38, 2001.

Liebe T. *Analytical and geometrical representation of localization analysis of curvilinear Drucker-Prager elastoplasticity*. Dipl. thesis, Technical report, University of Hanover, Germany, 1998.

Liebe T. and Willam K. Localization results of generalized Drucker-Prager elastoplasticity. *International Journal of Solids and Structures*, 127, 2001.

Lu X. *Uniaxial and triaxial behavior of high strength concrete with and without steel fibers*.

Ph.D. thesis, New Jersey Institute of Technology, 2005.

Nadai A. *Theory of Flow and Fractory of Solids*. Mc Graw, New York, 1950.

Oda M. and Kazama M. Microstructure of shear bands and its relation to the mechanisms of dilatancy and failure of dense granular soils. *Geotechnique*, 48:465–481, 1988.

Ottosen S. and Runesson K. Properties of discontinuous bifurcation solutions in elasto–plasticity. *International Journal of Solids and Structures*, 27:401–421, 1991.

Perić D. *Localized deformation and failure analysis of pressure sensitive granular materials*. University of Colorado, CEAE Dept., Boulder, USA, 1990.

Petersson P. *Crack growth and development of fracture zones in plain concrete and similar materials*. Report TVBM-1006. Technical report, Lund Institute of Technology, Sweden, 1981.

Phillips D.V. and Binsheng Z. Direct tension tests on notched and un-notched plain concrete specimens. *Mag. Concrete Res.*, 45:25–35, 1993.

Pijaudier-Cabot G. and Benallal A. Strain localization and bifurcation in a non-local continuum. *International Journal of Solids and Structures*, 13:1761–1775, 1993.

Planas J. and Elices M. *Towards a measure of G_f: An analysis of experimental results*. F.H. Wittmann, ed. Elsevier., 1986.

Planas J. and Elices M. *Conceptual and experimental problems in the determination of the fracture energy of concrete. Fracture Toughness and Fracture Energy: Test Methods for Concrete and Rock*. H. Mihashi, H.Takahashi and F.H. Wittmann, eds. Balkema., 1989.

Rizzi E. C.I. and Willam K. Localization analysis of elastic degradation with application to scalar damage. *J. Engng. Mech.*, 121, 1995.

Rudnicki J. and Rice J. Conditions for the localization of deformation in pressure-sensitive dilatant materials. *J. Mech. Phys. Solids*, 23:371–394, 1975.

Sfer D., Gettu R., Carol I., and Etse G. Experimental study of the triaxial behavior of concrete. *J. of Eng. Mech.*, 128, 2002.

Sobh N. *Bifurcation analysis of tangential material operators*. University of Colorado, CEAE Dept., Boulder, USA, 1987.

Thomas T. *Plastic flow and fracture in solids*. Academic Press, London, 1961.

van Geel X. *Concrete behaviour in multiaxial compression*. Ph.D. thesis, Technische Universiteit Eindhoven, Neatherlands, 1998.

van Mier J. *Strain-Softening of concrete under multiaxial loading conditions*. Ph. D. thesis, Eindhoven University of Technology, Neatherlands, 1984.

van Mier J. *Fracture processes of concrete*. CRC Press, 1997.

Vardoulakis I. Shear band inclination and shear modulus of sand in biaxial tests. *International Journal for Numerical and Analytical Methods in Geomechanics*, 4:103–119, 1980.

Vrech S. and Etse G. Geometrical localization analysis of gradient-dependent parabolic Drucker-Prager elastoplasticity. *International Journal of Plasticity*, 22:943–964, 2006.

Willam K. and Etse G. Failure assessment of the extended Leon model for plain concrete. *SCI-C Conf., Zell and See, Austria,Pineridge Press, Swansea, UK*, pages 851–870, 1990.